

Has the E791 experiment measured the pion wave function profile ?

Victor Chernyak

Budker Institute of Nuclear Physics,
630090 Novosibirsk, Russia

Abstract

The cross section of hard diffractive dissociation of the pion into two jets is calculated. It is obtained that the distribution of longitudinal momenta for jets is not simply proportional to the profile of the pion wave function, but depends on it in a complicated way. In particular, it is shown that, under the conditions of the E791 experiment, the momentum distribution of jets is similar in its shape for the asymptotic and CZ wave functions, and even the ratio of the differential cross sections is not far from unity.

We argue therefore that, unfortunately, the E791 experiment has not yet measured the profile of the pion wave function. For this, the experimental accuracy has to be increased essentially.

1. The E791 experiment at Fermilab [1] has recently measured the cross section of the hard diffractive dissociation of the pion into two jets. In particular, the distribution of the total pion longitudinal momentum into fractions y_1 and y_2 , $(y_1 + y_2) = 1$, between jets has been measured. The main purpose was to obtain in this way the information about the leading twist pion wave function $\phi_\pi(x_1, x_2)$, which describes the distribution of quarks inside the pion in the longitudinal momentum fractions x_1 and x_2 , $(x_1 + x_2) = 1$.

The hope was based on the theoretical calculations of this cross section in [2]-[4]. It has been obtained in all these papers that the cross section is simply proportional to the pion wave function squared: $d\sigma/dy_1 \sim |\phi_\pi(y_1)|^2$. In such a case, it would be sufficient to measure only the gross features of $d\sigma/dy$

to reveal the main characteristic properties of $\phi_\pi(x)$, and to discriminate between various available models of $\phi_\pi(x)$.

The purpose of this paper is to show that this is not the case. The real situation is much more complicated, with $d\sigma/dy$ depending on $\phi_\pi(x)$ in a highly nontrivial way. We give below (in a short form) the results of our calculation of this cross section.

2. The kinematics of the process is shown in fig. 1.

We take the nucleon as a target, and the initial and final nucleons are substituted by two soft gluons with momenta q_1 and q_2 . The lower blob in fig.1 represents the skewed gluon distribution of the nucleon, $g_\xi(u)$.

The final quarks are on shell, carry the fractions y_1 and y_2 of the initial pion momentum, and their transverse momenta are: $(\mathbf{k}_\perp + (\mathbf{q}_\perp/2))$ and $(-\mathbf{k}_\perp + (\mathbf{q}_\perp/2))$, $q_\perp \ll k_\perp$, where q_\perp is the small final transverse momentum of the target, while k_\perp is large.

The upper blob M in fig.1 represents the hard kernel of the amplitude which includes all hard propagators. For calculation of M in the leading twist approximation and in the lowest order in α_s , the massless pion can be substituted in all diagrams by two massless on shell quarks with the collinear momenta $x_1 p_\pi$ and $x_2 p_\pi$ and with zero transverse momenta, as account of primordial virtualities and transverse momenta results only in higher twist corrections to M . The leading twist pion wave function $\phi_\pi(x, \mu_o)$ describes the distribution of these quarks in momentum fractions x_1 and x_2 . ¹

The hard kernel M is proportional to the scattering amplitude of two initial collinear and on shell quarks of the pion on the on shell gluon:

$$d(x_1 p_\pi) + \bar{u}(x_2 p_\pi) + g(q_1) \rightarrow d(p_1) + \bar{u}(p_2) + g(q_2)$$

In lowest order in $\alpha_s(k_\perp)$ M consists of 31 connected Born diagrams, each one is $\sim O(\alpha_s^2(k_\perp))$ and contains exactly three hard propagators (except for one diagram with the 4-gluon vertex, which has only two). Two diagrams are represented explicitly in fig. 2 and fig. 3.

In the c.m.s. and to the leading twist accuracy, the initial and final soft gluons can be considered to be on shell, with transverse polarizations, carrying fractions $(u + \xi)$ and $(u - \xi)$ of the mean nucleon momentum \overline{P} .

¹ As usual, on account of leading logs from loops the soft pion wave function $\phi_\pi(x, \mu_o)$ evolves to $\phi_\pi(x, \mu) \sim \int^\mu d^2 l_\perp \Psi_\pi(x, l_\perp)$, where μ is the characteristic scale of the process. And the same for the gluon distribution: $g_\xi(u, \mu_o) \rightarrow g_\xi(u, \mu)$.

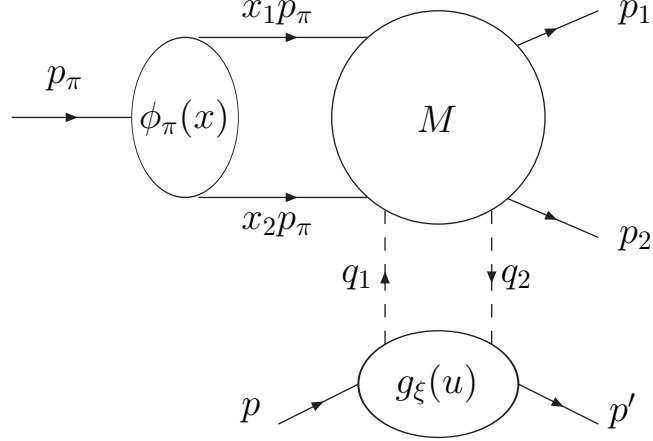


Figure 1: Kinematics and notations

² The nucleon can be considered as being massless, spinless, and its skewed gluon distribution $g_\xi(u, t, \mu_o) = g_\xi(-u, t, \mu_o)$, $-1 < u < 1$, is defined as ³ :

$$\begin{aligned} \langle P' | A_\lambda^{a,\perp}(v_1) A_\nu^{b,\perp}(v_2) | P \rangle_{\mu_o} &= -g_{\lambda\nu}^\perp \frac{\delta^{ab}}{8} \int_{-1}^1 \frac{du}{2} \frac{g_\xi(u, t, \mu_o)}{(u + \xi - i\epsilon)(u - \xi + i\epsilon)} \times \\ &\times \frac{1}{2} \left(e^{-i(u+\xi)(\bar{P}v_1) + i(u-\xi)(\bar{P}v_2)} + e^{-i(u+\xi)(\bar{P}v_2) + i(u-\xi)(\bar{P}v_1)} \right). \end{aligned} \quad (1)$$

This is equivalent to the standard definition (see [5-7]):

$$\begin{aligned} \langle P' | G_{\mu\lambda}^a(v_1) G_{\lambda\rho}^a(v_2) | P \rangle_{\mu_o} &= 2 \bar{P}_\mu \bar{P}_\rho \int_{-1}^1 \frac{du}{2} g_\xi(u, t, \mu_o) \times \\ &\times \frac{1}{2} \left(e^{-i(u+\xi)(\bar{P}v_1) + i(u-\xi)(\bar{P}v_2)} + e^{-i(u+\xi)(\bar{P}v_2) + i(u-\xi)(\bar{P}v_1)} \right). \end{aligned} \quad (2)$$

The kinematical variables are defined as:

$$q_1 = (u + \xi) \bar{P}, \quad q_2 = (u - \xi) \bar{P}, \quad \bar{P} = (P + P')/2,$$

² The small skewedness, $\xi \ll 1$, is always implied. It is typically: $\xi \sim 10^{-2}$, in the Fermilab experiment.

³ Here and below the gluon string is always implied in gauge invariant definitions of bilocal operators, both for the gluon distribution of the nucleon $g_\xi(u)$, and for the pion wave function $\phi_\pi(x)$.

$$\Delta = (q_1 - q_2) = 2\xi \overline{P}, \quad \xi = \frac{\mathbf{k}_\perp^2}{2y_1 y_2 s}, \quad z_1 = \frac{u + \xi}{2\xi}, \quad z_2 = \frac{u - \xi}{2\xi}, \quad (3)$$

$$z_1 - z_2 = 1, \quad 2(p_\pi \Delta) = M^2 = \frac{\mathbf{k}_\perp^2}{y_1 y_2}.$$

According to the well developed approach to description of hard exclusive processes in QCD [8]-[11] (see [12] for a review), all hard gluon and quark lines in all diagrams (see e.g. figs.2 and 3) have to be written down explicitly and substituted by their perturbative propagators. In other words, the hard momentum flow have to be made completely explicit and these hard lines of diagrams constitute the hard kernel M . They should not be hidden as (a derivatives of) "the tails" of the unintegrated pion wave function $\Psi_\pi(x, l_\perp)$, or of the "unintegrated gluon distribution". This is, first of all, what differs our approach from previous calculations of this process in [2-4] where, besides, most of diagrams were either ignored or calculated erroneously.⁴

Due to this the function $\Psi_\pi(x, l_\perp)$ (and the unintegrated gluon distribution) never appears explicitly in our calculations. It always enters the answer for each of 31 Born diagrams implicitly only through the function $\phi_\pi(x, \mu)$, i.e. only in the standard integrated form: $\phi_\pi(x, \mu) \sim \int^\mu d^2 l_\perp \Psi_\pi(x, l_\perp)$.⁵

So, the structure of the amplitude is (symbolically):

$$T \sim \langle P' | A^\perp \cdot A^\perp | P \rangle \otimes (\bar{\psi}_1 M \psi_2) \otimes \langle 0 | \bar{u} \cdot d | \pi^- \rangle, \quad (4)$$

where the first matrix element introduces the skewed gluon distribution of the nucleon $g_\xi(u)$, $\bar{\psi}_1$ and ψ_2 are the free spinors of final quarks, "M" is the

⁴ While a small number out the whole set of 31 diagrams can possibly be reinterpreted through "the tails" of the unintegrated pion wave function $\Psi_\pi(x, l_\perp)$ or of the "unintegrated gluon distribution", this is definitely not the case for most of diagrams. So, we see no much meaning to proceed in this way.

In a sense, the contribution of each diagram is essential in obtaining the numerical description for the "y"-distribution of jets in sect.4. In our approach all 31 diagrams are treated on equal footing.

⁵ In [3] the authors tried to use the evolution equation for the pion wave function to obtain its "tail". For instance, for the asymptotic wave function it was obtained in this way: $\Psi_\pi^{asy}(x, k_\perp) \sim \phi_\pi^{asy}(x, \mu)/k_\perp^2$. It remains unclear for us how it is possible to obtain such a result from the evolution equation for the asymptotic wave function which looks as: $d\phi_\pi^{asy}(x, \mu)/d \ln \mu = \int dy V(x, y) \phi_\pi^{asy}(y, \mu) = 0$.

hard kernel, i.e. the product of all vertices and hard propagators, the last matrix element introduces the pion wave function $\phi_\pi(x)$, and \otimes means the appropriate convolution.

As an example, let us consider the diagram in fig. 2. Proceeding in the above described way (see the appendix), one obtains the contribution to the amplitude (the Feynman gauge is used for the hard gluon):

$$T_2 = -\frac{16}{9} \frac{\omega_o}{y_2} \int_0^1 \frac{dx_1 \phi_\pi(x)}{x_1 x_2} \int_{-1}^1 \frac{du g_\xi(u)}{(u - \xi)(u + \xi)}, \quad (5)$$

$$\omega_o = \delta_{ij} \frac{(4\pi\alpha_s)^2}{96} f_\pi (\bar{\psi}_1 \hat{\Delta} \gamma_5 \psi_2) \frac{(y_1 y_2)^2}{k_\perp^4}, \quad \hat{\Delta} = \Delta_\mu \gamma_\mu, \quad (6)$$

where $\bar{\psi}_1$ and ψ_2 are the free spinors of the final quarks, $\Sigma_{spins} |\bar{\psi}_1 \hat{\Delta} \gamma_5 \psi_2|^2 = 2 k_\perp^4 / (y_1 y_2)$, "ij" are their colour indices, and $f_\pi \simeq 130 \text{ MeV}$ is the pion decay constant.

As it is expected that, for this process, the imaginary part of the amplitude is the main one at high energy, we show explicitly in ch.3 only its value. For the diagram in fig. 2 this gives (in all diagrams the terms $i\epsilon$ are introduced into denominators through $s \rightarrow s + i\epsilon$, i.e. $\xi \rightarrow \xi - i\epsilon$):

$$\text{Im } T_2 = \frac{16}{9} \frac{2\pi s \omega_o y_1}{k_\perp^2} g_\xi(\xi) \int_0^1 \frac{dx_1 \phi_\pi(x)}{x_1 x_2}. \quad (7)$$

As a final example, let us also consider the diagram in fig. 3, as it gives (together with the mirror diagram obtained by $q_1 \leftrightarrow q_2$) the enhanced contribution⁶:

$$T_3 = \frac{\omega_o}{y_1 y_2} \int_0^1 \frac{dx_1 \phi_\pi(x)}{x_1 x_2} \int_{-1}^1 \frac{du g_\xi(u) N}{(u - \xi)(u + \xi)[z_1(x_1 - y_1) - x_1 y_2]}, \quad (8)$$

$$N = [-8 z_1 z_2] + (8 y_1 y_2 - 3 - x_1 y_1 - x_2 y_2) + (z_1 + z_2)(x_1 - y_1), \quad (9)$$

$$\text{Im } T_3 = 8 \frac{\pi s \omega_o}{k_\perp^2} \int_0^1 \frac{dx_1 \phi_\pi(x) g_\xi(\bar{u})}{x_1 x_2 |x_1 - y_1|} \Theta(|x_1 - y_1| > \delta) + \dots, \quad (10)$$

⁶ The analytic form of the enhancement depends on the behaviour of the gluon distribution $g_\xi(u)$, see eq.(10). With $g_\xi(u) \sim \text{const}$ the enhancement is logarithmic, $\sim \ln(s/k_\perp^2)$, but with $g_\xi(u)$ from eq.(18) it is only numerical.

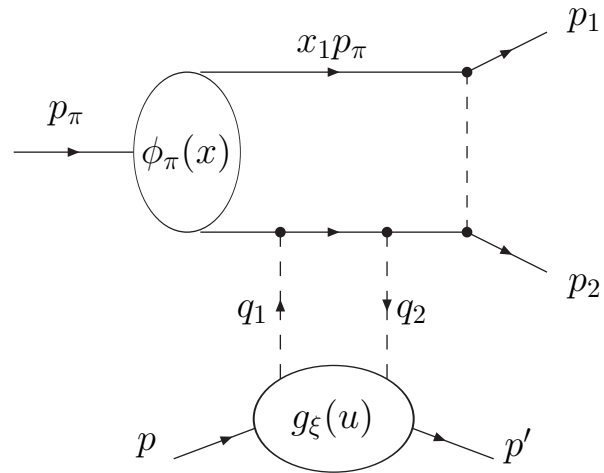


Figure 2: One of the diagrams

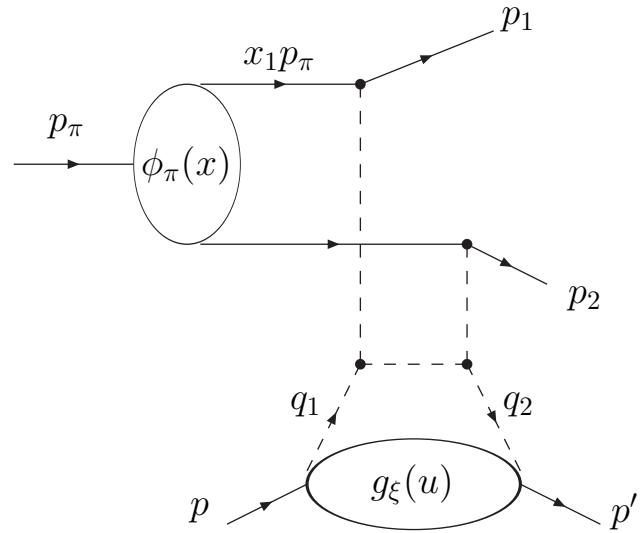


Figure 3: The diagram giving the enhanced contribution

$$\bar{u} = \xi \left(\frac{x_1 y_2 + x_2 y_1}{x_1 - y_1} \right), \quad \delta = k_\perp^2/s, \quad (11)$$

where only the enhanced term is shown explicitly in eq.(10), which originates from the term in square brackets in eq.(9). ⁷

3. Proceeding in the above described way and summing up the contributions of all 31 Born diagrams, one obtains for the cross section:

$$d\sigma_N = \frac{1}{8(2\pi)^5} \frac{1}{s^2} |T|^2 \frac{dy_1}{y_1 y_2} d^2 k_\perp d^2 q_\perp, \quad T \simeq i \operatorname{Im} T = i \frac{2\pi s \omega_o}{k_\perp^2} g_\xi(\xi) \Omega, \quad (12)$$

$$\Omega = \int_0^1 dx_1 \phi_\pi(x_1) (\Sigma_1 + \Sigma_2 + \Sigma_3 + \Sigma_4), \quad (13)$$

$$\Sigma_1 = \left[\frac{4}{x_1 x_2 |x_1 - y_1|} \frac{g_\xi(\bar{u})}{g_\xi(\xi)} \Theta(|x_1 - y_1| > \delta) \right] + (y_1 \leftrightarrow y_2), \quad (14)$$

$$\begin{aligned} \Sigma_2 = & \frac{1}{x_1^2 x_2^2 y_1 y_2} \left\{ -(x_1 x_2 + y_1 y_2) + \right. \\ & \left. + \left[|x_1 - y_1| (x_1 - y_2)^2 \frac{g_\xi(\bar{u})}{g_\xi(\xi)} \Theta(|x_1 - y_1| > \delta) + (y_1 \leftrightarrow y_2) \right] \right\}, \end{aligned} \quad (15)$$

$$\Sigma_3 = \frac{1}{9} \left(\frac{x_1 x_2 + y_1 y_2}{x_1^2 x_2^2 y_1 y_2} \right) \left\{ -1 + \left[|x_1 - y_1| \frac{g_\xi(\bar{u})}{g_\xi(\xi)} \Theta(|x_1 - y_1| > \delta) + (y_1 \leftrightarrow y_2) \right] \right\}, \quad (16)$$

$$\Sigma_4 = \frac{16}{9} \frac{1}{x_1 x_2 y_1 y_2} \xi \frac{dg_\xi(u)/du|_{u=\xi}}{g_\xi(\xi)}. \quad (17)$$

The expressions (12)-(17) constitute the main result of this paper.

⁷ As the Θ - function in eq.(10) excludes the region of x_1 too close to y_1 , the integral is convergent and only some enhancement remains (see the footnote 6).

At the conditions of the E791 experiment (and even at much larger energies, see fig.6), this enhancement is by no means sufficient to neglect contributions of all other diagrams.

Let us note that while the separate terms in $\int dx \phi_\pi(x) \Sigma_2$ are logarithmically divergent at $x_{1,2} \rightarrow 0$, it is not difficult to see that the divergences cancel in the sum, so that the integral is finite. And the same is valid for Σ_3 . This is an important point as it shows that the whole approach is self-consistent, i.e. the hard kernel remains hard and the soft end point regions $x_{1,2} \rightarrow 0$ give only power suppressed corrections.

4. In this section we present some numerical estimates of the cross section, based on the above expressions (12)-(17). Our main purpose here is to trace the distribution of jets in longitudinal momentum fractions y_1, y_2 depending on the profile of the pion wave function $\phi_\pi(x)$.

a) As the calculations were performed in the leading twist approximation which becomes applicable at sufficiently large k_\perp only, we take $k_\perp = 2 \text{ GeV}$. This assumes that the higher twist effects are not of great importance at such a value of k_\perp , and gives a possibility of comparison with the E791-data.

b) For the skewed gluon distribution $g_\xi(u, t, \mu)$ of the nucleon at $t \simeq -q_\perp^2 \simeq 0$ we use the simple form (as we need it at $|u| \geq \xi$ only, and because $g_\xi(u) \rightarrow g_o(u)$ at $|u| \gg \xi$):

$$g_\xi(u, t = 0, \mu \simeq k_\perp \simeq 2 \text{ GeV})|_{u \geq \xi} \simeq u^{-0.3}(1 - u)^5. \quad (18)$$

This form agrees numerically reasonably well with the ordinary, $g_o(u, \mu \simeq 2 \text{ GeV})$, and skewed, $g_\xi(u, t = 0, \mu \simeq 2 \text{ GeV})$, gluon distributions of the nucleon calculated in [13] and [14] respectively (in the typical region of the E791 experiment: $|u| \geq \xi \sim 10^{-2}$).

The detailed consideration of nuclear effects is out the scope of this paper. So, we simply assume that these effects result mainly in an overall factor (see [3]):

$$d\sigma_A(t \simeq -q_\perp^2) \simeq d\sigma_N(t = 0) |A F_A(t)|^2, \quad (19)$$

where $F_A(t) = \exp\{bt/2\}$, $b = \langle R_A^2 \rangle/3$, is the nuclear form factor.

c) As for the pion leading twist wave function, $\phi_\pi(x, \mu)$, we compare two model forms: the asymptotic form, $\phi_\pi^{asy}(x, \mu) = 6x_1x_2$, and the CZ-model [15]. The latter has the form: $\phi_\pi^{CZ}(x, \mu_o \simeq 0.5 \text{ GeV}) = 30x_1x_2(x_1 - x_2)^2$, at the low normalization point. Being evolved up to the characteristic scale $\mu \simeq k_\perp \simeq 2 \text{ GeV}$, it looks as⁸ (see fig. 4):

$$\phi_\pi^{CZ}(x, \mu \simeq 2 \text{ GeV}) = 15x_1x_2[(x_1 - x_2)^2 + 0.2]. \quad (20)$$

⁸ As the final quarks are free, the wave function of this two quark system is the asymptotic one, and it does not evolve in the leading log approximation.

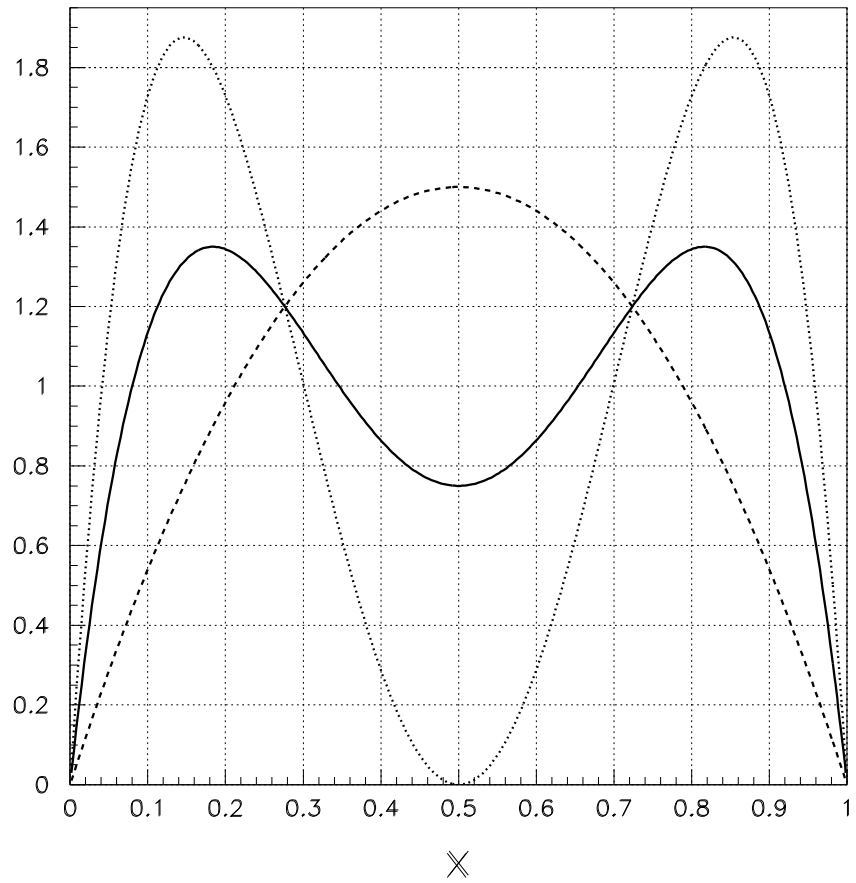


Figure 4: Profiles of the pion wave functions: a) $\phi_{\pi}^{CZ}(x, \mu \simeq 0.5 \text{ GeV}) = 30 x_1 x_2 (x_1 - x_2)^2$ - dotted line; b) $\phi_{\pi}^{CZ}(x, \mu \simeq 2 \text{ GeV}) = 15 x_1 x_2 [0.2 + (x_1 - x_2)^2]$ - solid line; c) $\phi_{\pi}^{asy}(x) = 6 x_1 x_2$ - dashed line.

The results of these numerical calculations are then compared with the E791-data, see fig. 5.

It is seen that, unfortunately, while two pion wave functions are quite different, the resulting distributions of jets in longitudinal momenta are similar and, it seems, the present experimental accuracy is insufficient to distinguish clearly between them. Moreover, even the ratio of the differential cross sections is not much different from unity: $d\sigma^{asy}/d\sigma^{CZ} \simeq 1.2$ at $y_1 = 0.5$, and the same ratio is $\simeq 0.7$ at $y_1 = 0.25$.

In such an unhappy situation, the theoretical calculations should be also performed with a maximal possible accuracy (to account additionally for: the quark distributions, higher twist corrections, hard loop corrections, nuclear effects etc.).

We also show in fig. 6 the same distributions with the pion energy ten times larger, $E_\pi = 5 \text{ TeV}$, $k_\perp = 2 \text{ GeV}$. It is seen that even this does not help much (as the form of the distribution weakly depends on the pion energy). The same ratios of the cross sections are here $\simeq 1.7$ and $\simeq 0.7$ respectively.

Recently the Coulomb contribution to the cross section has been calculated in [16].⁹ Its value for P_t is: $d\sigma_{P_t}^{electr}/dk_\perp^2 dy < 10^{-5} \text{ mbarn} \cdot \text{GeV}^{-2}$, for $E_\pi = 500 \text{ GeV}$, $k_\perp = 2 \text{ GeV}$. Using the above given formulae, one obtains for the strong cross section at the middle point $y = 0.5$: $d\sigma_{P_t}^{CZ}/dk_\perp^2 dy \simeq 2.5 \cdot 10^{-2} \text{ mbarn} \cdot \text{GeV}^{-2}$ with the same parameters, and $\simeq 0.25 \text{ mbarn} \cdot \text{GeV}^{-2}$ at $E_\pi = 5 \text{ TeV}$. It is seen that the electromagnetic contribution is small.

Note added: After this work has been completed, the paper [17] on the same subject appeared. Comparison shows that, although the qualitative conclusions are similar, the analytic expressions for the scattering amplitude differ essentially in this paper and in [17].¹⁰

Acknowledgements

I am grateful to V.S. Fadin for useful discussions and critical remarks. I also thank A.E. Bondar and B.I. Khazin for explaining me some details of the E791 experiment.

⁹ Since the electromagnetic contribution is real while the strong one is mainly imaginary, they do not interfere.

¹⁰ In comparison with their original calculation the authors of [17] have found recently an additional missed contribution, so that their revised analytic results for the amplitude agree now with those obtained in this paper, see eqs.(12-17).

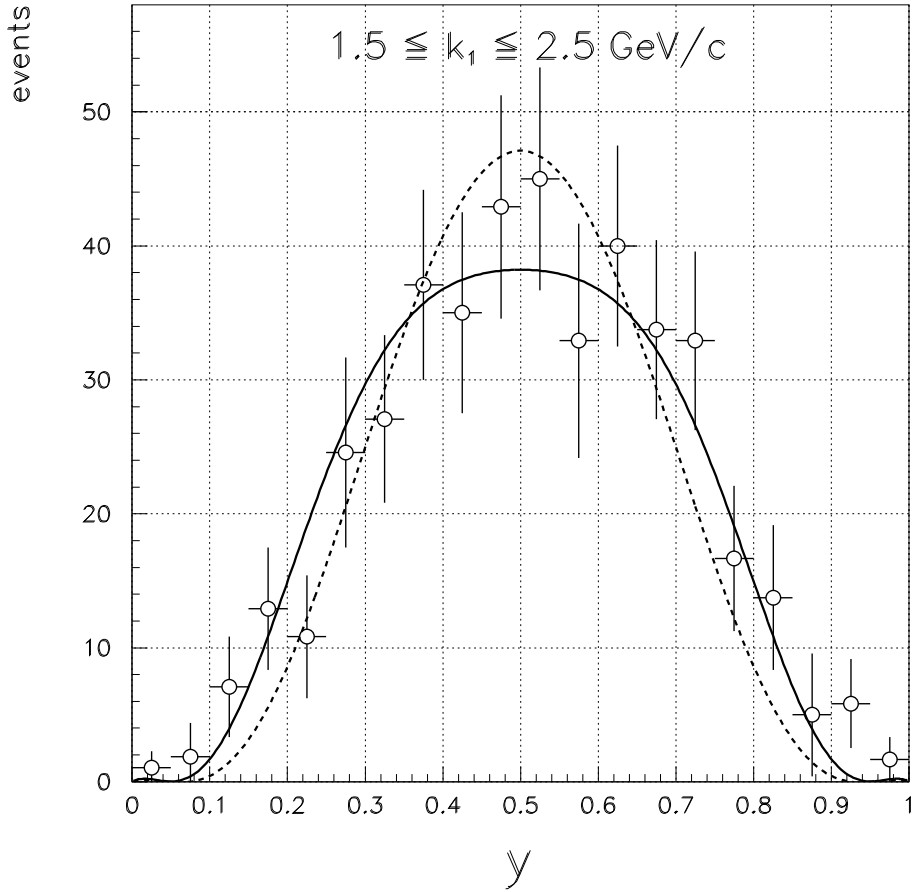


Figure 5: The y -distribution of jets calculated for $k_{\perp} = 2 \text{ GeV}$, $E_{\pi} = 500 \text{ GeV}$ and with the pion wave functions: $\phi_{\pi}^{CZ}(x, \mu \simeq 2 \text{ GeV})$ - solid line, $\phi_{\pi}^{asy}(x)$ - dashed line. The overall normalization is arbitrary, but the relative normalization of two curves is as calculated. The data points are from the E791 experiment [1].

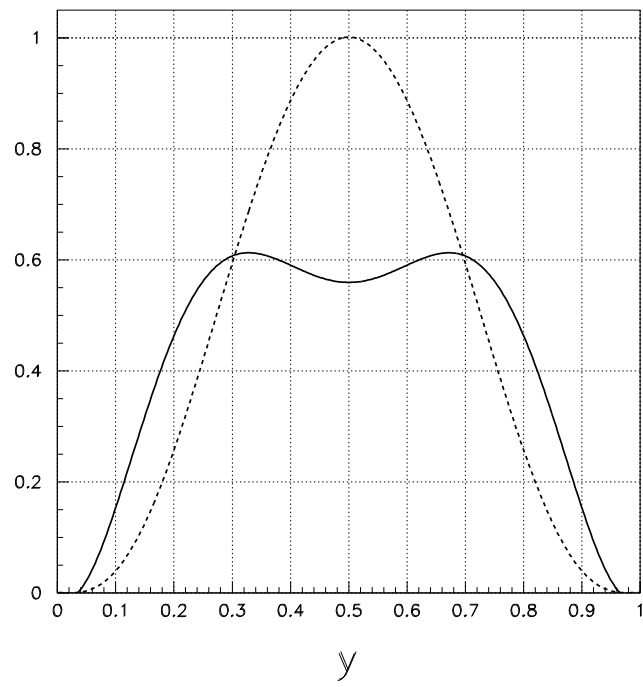


Figure 6: The same as in Fig.5, but with $E_\pi = 5 \text{ TeV}$.

Appendix

The purpose of this appendix is to give (somewhat schematically) some details of how the diagrams have been calculated. As an example, let us consider the simplest diagram in fig.2. The momentum of the virtual gluon is: $k = (x_1 p_\pi - p_1)$. The momenta of virtual quarks are: $\sigma = (-x_2 p_\pi - z_1 \Delta)$ and $\rho = (-x_2 p_\pi - \Delta)$, with $q_{1,2} = z_{1,2} \Delta$, see eq.(3). The overall denominator is therefore: $D = k^2 \sigma^2 \rho^2 = (-x_1 x_2^2 y_2 z_1)(2p_\pi \Delta)^3$. This diagram looks (in the operator form) as:

$$T_2 = i \frac{(4\pi\alpha_s)^2}{D} \left[\bar{d} \frac{\lambda^a}{2} \gamma_\mu d \right] \left[\bar{u} \frac{\lambda^b}{2} \gamma_\lambda \hat{\sigma} \frac{\lambda^c}{2} \gamma_\nu \hat{\rho} \frac{\lambda^a}{2} \gamma_\mu u \right] \left[A_\lambda^{\perp,b} A_\nu^{\perp,c} \right]. \quad (21)$$

The matrix element of this operator between the initial and final states is factorized then into three parts. The first part is the matrix element of the gluon fields between the initial and final nucleons, this introduces the gluon distribution, see eq.(1):

$$\langle P' | A_\lambda^{\perp,b} A_\nu^{\perp,c} | P \rangle \rightarrow -g_{\lambda\nu}^\perp \frac{\delta^{bc}}{8} \frac{g_\xi(u)}{4(u-\xi)(u+\xi)}. \quad (22)$$

The second part is the matrix element of two quark fields $d_\alpha^k \bar{u}_\beta^l$ between the pion and vacuum, this introduces the pion wave function ¹¹:

$$\langle 0 | d_\alpha^k \bar{u}_\beta^l | \pi^- \rangle \rightarrow \frac{\delta^{kl}}{3} \frac{(\hat{p}_\pi \gamma_5)_{\alpha\beta}}{4} i f_\pi \phi_\pi(x). \quad (23)$$

The last part is the matrix element of two remaining quark fields between the vacuum and the final state of two free quarks. This introduces the Dirac spinors $\bar{\psi}_1$ and ψ_2 . The result is integrated then over "x" and "u". So, one obtains:

$$T_2 = \int_0^1 dx_1 \int_{-1}^1 du (4\pi\alpha_s)^2 \frac{f_\pi \phi_\pi(x)}{12} \frac{g_\xi(u)}{32(u-\xi)(u+\xi)} \left(\frac{4}{3} \right)^2 \delta_{ij} (\bar{\psi}_1 M \psi_2), \quad (24)$$

$$(\bar{\psi}_1 M \psi_2) = \frac{1}{D} (\bar{\psi}_1 \gamma_\mu \hat{p}_\pi \gamma_5 \gamma_\lambda^\perp \hat{\sigma} \gamma_\lambda^\perp \hat{\rho} \gamma_\mu \psi_2) = 4 x_2 z_1 \frac{(2p_\pi \Delta)}{D} (\bar{\psi}_1 \hat{\Delta} \gamma_5 \psi_2). \quad (25)$$

On the whole, one obtains the eqs.(5,6). All other 30 diagrams have been calculated in the same way.

¹¹ Eq.(23) is a shorthand for a standard definition of the pion wave function $\phi_\pi(x)$ through the matrix element of the gauge invariant bilocal quark operator, see [8, 9], in the same way as eq.(22) is a shorthand for eq.(1). See also the footnote 3.

References

- [1] E.M. Aitala et. al. (E791 Collaboration), hep-ex/**0010043**
D. Ashery, hep-ex/**9910024**; Invited Talk at X Intern. Light-Cone
Meeting, Heidelberg, June 2000: hep-ex/**0008036**
- [2] G. Bertsch, S.J. Brodsky, A.S. Goldhaber and J.G. Gunion,
Phys. Rev. Lett. **47** (1981) 297
- [3] L. Frankfurt, G.A. Miller and M. Strikman, Phys. Lett. **B304** (1993) 1;
Found. of Phys. **30** (2000) 533 (hep-ph/**9907214**); hep-ph/**0010297**
- [4] N.N. Nikolaev, W. Schafer and G. Schwiete, Phys. Rev. **D63** (2001)
014020; hep-ph/**009038**
- [5] D. Muller, D. Robaschik, B. Geyer, F.-M. Dittes and J. Horejsi,
Forts. Phys. **42** (1994) 101
- [6] A.V. Radyushkin, Phys. Lett. **B385** (1996) 333; Phys. Rev. **D56** (1997)
5524
- [7] X. Ji, Phys. Rev. Lett. **78** (1997) 610; J. Phys. **G24** (1998) 1181
- [8] V.L. Chernyak and A.R. Zhitnitsky, JETP Lett. **25** (1977) 510; Sov. J.
Nucl. Phys. **31** (1980) 544
- [9] V.L. Chernyak, V.G. Serbo and A.R. Zhitnitsky, JETP Lett. **26** (1977)
594; Sov. J. Nucl. Phys. **31** (1980) 552
- [10] A.V. Efremov and A.V. Radyushkin, Phys. Lett. **B94** (1980) 245;
Teor. Math. Phys. **42** (1980) 97
- [11] G.P. Lepage and S.J. Brodsky, Phys. Lett. **B87** (1979) 359; Phys. Rev.
D22 (1980) 2157
- [12] V.L. Chernyak and A.R. Zhitnitsky, Phys. Rep. **112** (1984) 173
- [13] M. Gluck, E. Reya and A. Vogt, Eur. Phys. J. **C5** (1998) 461
- [14] K.J. Golec-Biernat, A.D. Martin and M.G. Ryskin,
Phys. Lett. **B456** (1999) 232; hep-ph/**9903327**
- [15] V.L. Chernyak and A.R. Zhitnitsky, Nucl. Phys. **B201** (1982) 492

- [16] D.Yu. Ivanov and L. Szymanowski, hep-ph/**0103184**
- [17] V.M. Braun, D.Yu. Ivanov, A. Schafer and L. Szymanowski, hep-ph/**0103275**; Phys. Lett. **B509** (2001) 43